Published in final edited form as:
Calcif Tissue Int. 2014 May ; 94(5): 544–552. doi:10.1007/s00223-014-9839-6.

A Dual Isotope Hybrid Whole Body Micro-PET/CT System Reveals Functional Heterogeneity and Early Local and Systemic Changes Following Targeted Radiation to the Murine Caudal Skeleton

Masashi Yagi, MSc[1,2], **Luke Arentsen, BSc**[1], **Ryan M. Shanley, MSc**[3], **Clifford J. Rosen, MD**[4], **Louis S. Kidder, PhD**[1], **Leslie C. Sharkey, DVM, PhD**[5], **Douglas Yee, MD**[6,7], **Masahiko Koizumi, MD, PhD**[8], **Kazuhiko Ogawa, MD, PhD**[2], and **Susanta K. Hui, PhD**[1,7]

[1]Department of Therapeutic Radiology, Medical School, University of Minnesota, Minneapolis, Minnesota, United States of America

[2]Department of Radiation Oncology, Osaka University Graduate School of Medicine, Suita, Osaka, Japan

[3]Biostatistics Core, Masonic Cancer Center, University of Minnesota, Minneapolis, Minnesota, United States of America

[4]Maine Medical Center Research Institute, Scarborough, Maine, United States of America

[5]Department of Veterinary Clinical Sciences, College of Veterinary Medicine, University of Minnesota, St. Paul, Minnesota, United States of America

[6]Department of Medicine, Medical School, University of Minnesota, Minneapolis, Minnesota, United States of America

[7]Masonic Cancer Center, University of Minnesota, Minneapolis, Minnesota, United States of America

[8]Department of Medical Physics and Engineering, Osaka University Graduate School of Medicine, Suita, Osaka, Japan

Abstract

The purpose of this study is to develop a longitudinal non-invasive functional imaging method using a dual isotope hybrid micro-PET/CT scanner in order to assess both the skeletal metabolic heterogeneity and the effect of localized radiation that models therapeutic cancer treatment on marrow and bone metabolism. Skeletally mature BALB/c female mice were given clinically relevant local radiation (16 Gy) to the hind limbs on day 0. Micro-PET/CT acquisition was performed serially for the same mice on days -5 and +2 with FDG and days -4 and +3 with NaF. Serum levels of pro-inflammatory cytokines were measured. Significant differences ($p<0.0001$) in marrow metabolism (measured by FDG) and bone metabolism (measured by NaF) were observed

Address for correspondence: Susanta K Hui, PhD, DABR, Department of Therapeutic Radiology, University of Minnesota, 420 Delaware Street SE, Mayo Mail Code 494, Minneapolis, MN 55455, Phone: 612-626-4484, Fax: 612-626-7060; huixx019@umn.edu.

Conflicts of interest
The authors declare that they have no conflict of interest.

among bones before radiation which demonstrates functional heterogeneity in the marrow and mineralized bone throughout the skeleton. Radiation significantly ($p<0.0001$) decreased FDG uptake but increased NaF uptake ($p=0.0314$) in both irradiated and non-irradiated bones at early time points. An increase in IL-6 was observed with a significant abscopal (distant) effect on marrow and bone metabolic function. Radiation significantly decreased circulating IGF-1 ($p<0.01$). Non-invasive longitudinal imaging with dual isotope micro-PET/CT is feasible to investigate simultaneous changes in marrow and bone metabolic function in local and distant skeletal sites in response to focused radiation injury. Distinct local and remote changes may be affected by several cytokines activated early after local radiation exposure. This approach has the potential for longer term studies to clarify the effects of radiation on marrow and bone.

Keywords

translational research; radiotherapy; micro-PET/CT; bone

Introduction

With increased cancer survivorship [1], there is an increased and unmet need to evaluate treatment-related skeletal damage, including the understanding of mechanisms of damage that will lead to preventive strategies. Skeletal damage and response to treatments are regionally variable [2–4], however, published reports have investigated only specific bone regions and fail to take a comprehensive approach. Our recent mouse micro-computed tomography (CT) study revealed the potential for anatomical heterogeneity in the whole skeleton [5]. Most preclinical experimental approaches are invasive and do not support the longitudinal experimental designs that are preferable to document changes over time within individuals. Other non-invasive options for hematopoietic and skeletal assessment include measuring plasma concentrations of Flt-3 ligand [6] and ^{45}Ca assays for bone remodeling [7], respectively. However, these methods only provide a measure of global damage. Characterization of regional marrow and bone metabolism are required to understand local and global tissue environments and treatment responses with emphasis on regions at risk for the development of metastatic disease and pathologic fractures [8].

Advancing the care of cancer patients requires the development and validation of appropriate experimental systems to ensure that animal studies accurately simulate clinical applications of radiotherapy based on radiobiologically relevant dose selection [9,7]. Monitoring the local and systemic changes in bone remodeling and skeletal damage resulting from local radiation will be bene cial for optimizing potential interventions proceeding cancer therapy. Furthermore, a recent study strongly supports bidirectional co-regulation of marrow and bone at the microenvironment level [10]. Thus, a comprehensive approach to understanding the integrated response of both marrow and bone tissue to radiation damage is necessary. Taking advantage of novel non-invasive micro-CT guided micro-positron emission tomography (PET) in a hybrid system and dual tracers (^{18}F labeled fluoro-2-deoxy-2-D-glucose (FDG), ^{18}F labeled sodium fluoride (NaF)), we investigated functional heterogeneity of the whole skeleton and then examined the early effects of a

clinically relevant local radiation application on local and systemic marrow and bone in an *in vivo* model longitudinal study.

Methods and Materials

Regulatory compliance

All animal studies were approved by the Institutional Animal Care and Use Committee (IACUC) at University of Minnesota.

Subjects

Six 16 week-old healthy BALB/c female mice (19.7±1.8 g, Harlan Sprague Dawley, Inc., Madison, WI, USA) were used for this study. All rodents were kept in a standard vivarium and were fed regular mouse diet and water ad libitum. All mice were fasted for at least 1.5 hours before isotope injection.

Radiation delivery

The XRad 320 Biological Irradiator (Precision X-Ray, Inc., North Branford, CT, USA) was used for all irradiation procedures. Under anesthesia (IP injection with ketamine/xynazine cocktail), a specially designed lead shield (4 mm thickness) was placed over the body, to limit exposure to only the hind limbs (Fig. 1A). Total dose delivered(16 Gy single fraction) and skeletal volume irradiated were equivalent to pelvic irradiation based on normalized total dose (NTD) [11] as previously described by Hui et al with details of verifications [9,7].

PET image acquisition

PET acquisition was performed serially on days -5 and +2 with FDG for marrow metabolism [12] and days -4 and +3 with NaF for bone metabolism [13] relative to radiation treatment in the same mice (Fig. 1B). The Inveon™ (Siemens Medical Solutions, Knoxville, TN, USA) scanned the region from skull to tibia. The isotopes were injected intravenously via the tail vein. The mean dose of FDG and NaF in 100 μl solution were 18.9±1.6 and 18.8±2.7 MBq, respectively, and measured with Atomlab 100 (Biodex Medical, Shirley, NY, USA), that had been cross-calibrated with the scanner. The 30 minute scan (list-mode data acquisition) was started at 30 minutes post-injection under anesthesia using the manufacture's recommended acquisition settings. For scanning, anesthesia was maintained at 1.5–3% isoflurane in 1 l/min O_2 via nose cone. During the scan, the mouse was monitored with a dedicated respiration monitor (BioVet, Spin Systems Pty Ltd., Brisbane, Australia). A dedicated warming pad and infrared thermometer were also used to maintain body temperature. Legs were taped to minimize the movement.

Inveon acquisition workplace software (IAW, version 1.5.0.28, Siemens Medical Solutions) was used for PET image reconstruction. The 30 minute acquisition was separated into three frames, each 600 seconds, with a 128 × 128 × 159 matrix (pixel size: 0.776 mm; plane thickness: 0.796 mm). After identifying the plateau region, the last 10 minute frame in the list-mode data (i.e. the last frame) was used. OSEM3D (ordered subset expectation maximization)/MAP (maximum a posteriori) algorithm with default parameters was employed for image reconstruction. Scatter and attenuation corrections were applied. For

anatomy registration, PET images were fused with CT image through a spatial transformation matrix which had been calibrated in the system setup. The micro-PET/CT system uses analytic rigid-body registration algorithm based on singular value decomposition to create the transformation matrix [14].

Blood sampling

Venous blood was collected in pre-weighed heparinized capillary tubes following the scan. The filled tube was weighed and the bottom sealed with capillary wax. Isotope activity was then counted with a well counter (ST360W radiation counter, Spectrum Techniques, Inc., Oak Ridge, TN, USA) and normalized to blood volume.

Image analysis

Scan analyses were performed using PMOD software version 3.4, build 6 (PMOD Technologies, Ltd., Zurich, Switzerland). The bone VOIs (volume of interest) were first drawn on the CT image and later exported to the PET image. Contouring was done by one investigator (M.Y.) and VOIs were identified semi-automatically using the segmentation feature based on a 3D region-growing algorithm and manual modification to minimize variations. There are eight regions; skull, mandible, humerus, cervical spine, thoracic spine (5th–10th), lumbar spine (1st–3rd), femur and tibia (40 slices from knee joint). The activity concentrations in the PET image and blood activity concentrations were corrected for radiotracer decay (109.77 minutes) back to the tracer injection time. Whole blood and plasma activities approached steady-state at 60 minutes after injection (FDG: [15], NaF: [16]). Thus, whole blood can be used as a surrogate for plasma activity. A recovery coefficient was not applied. The activity ratios of skeletal regions to blood were calculated as bone-to-blood ratios. There is no unit of uptake of tracer because the value is calculated as ratio of bone uptake activity (kBq/ml) to blood activity (kBq/ml). Heterogeneity is described as a varying uptake distribution of tracer among skeletal sites in this study.

Measurements of pro-inflammatory markers

An additional seven mice were used as for cytokine measurements. Post-mortem cardiac puncture blood samples were obtained. Serum interferon gamma (IFNγ), interleukin-10 (IL-10), interleukin-12p70 (IL-12p70), interleukin-1 beta (IL-1β), interleukin-6 (IL-6), tumor necrosis factor alpha (TNFα) and chemokine (C-X-C motif) ligand 1 (CXCL 1) levels were measured using the Mouse ProInflammatory 7-Plex Ultra-Sensitive Kit (Meso Scale Discovery, Gaithersburg, MD, USA) according to the manufacturer's instructions. Assay sensitivities were 0.38, 11, 35, 0.75, 4.5, 0.85, and 3.3 pg/ml, respectively. The intra-assay and inter-assay variations were less than 10% for all markers. Serum insulin-like growth factor 1 (IGF-1) levels were measured using a kit (IDS, Fountain Hills, AZ, USA) according to the manufacturer's instructions. Assay sensitivity was 2.8 ng/ml. Intra- and inter-assay variation were 5.8% and 7.8%, respectively. All measurements were performed in duplicate.

Statistical analysis

Changes in FDG and NaF before and after radiation were analyzed by mixed effects ANOVA, using SAS proc mixed (version 9.2, SAS Institute, Inc.). The models included

fixed effects for body region, radiation, their interaction, and a random mouse effect to account for correlation between pre and post-radiation measurements on the same mouse. Outcome variables (normalized blood) were log-transformed to give a multiplicative rather than additive model; that is, the effect of radiation on outcomes was modeled as a relative change rather than absolute. Model contrasts were used to estimate the magnitude of the radiation effect in each region and its interaction with other regions. Two-sided t-tests with unequal variance assessed differences in mean cytokine levels between control and radiation group.

Results

Figure 2 shows whole body scans of FDG (A and B) and NaF (C and D) uptake before and after radiation, demonstrating functional heterogeneity and radiation effect on bone.

Functional heterogeneity in the whole skeleton

FDG and NaF uptake are significantly different among bone regions (blue bars in Figs. 2E and F, $p<0.0001$ for FDG and NaF). Cervical and lumbar vertebrae had the highest uptake in both FDG and in NaF, respectively. Tibia exhibited the lowest uptake of both.

Radiation effect on bone

Radiation exposure to the hind limbs was 16.98±1.58 Gy. Visually, there was differential tracer uptake (Fig. 2). Quantitatively, the degree of uptake after radiation exposure differed among the regions ($p=0.0002$, Table 1). Irradiated region, especially the tibia, demonstrated significantly reduced FDG uptake at 32% of pre-radiation levels. Thoracic vertebrae were higher and tibia was lower compared with an overall average reduction ($p<0.01$, Table 1). Fig. 3A shows FDG uptake averaged over all bone regions, demonstrating that radiation decreased FDG uptake overall ($p<0.0001$) on day 2 after radiation. Despite individual variability, uptake after radiation was approximately 50% of pre-radiation levels (Table 1). Figure 3B shows the difference in FDG uptake of individual mice before and after radiation. All mice show a similar response pattern with high activity in the skull and spine but with large variations (coefficient of variation) between individuals. In contrast, radiation significantly suppressed metabolic activity in the entire skeleton in all subjects with minimal individual variation.

Red bars in Fig. 2F show NaF uptake following radiation. In individual mice, the NaF uptake averaged over all regions increased by a factor of 2.2. The degree of uptake after radiation differed among the regions ($p=0.0003$, Table 1). The mandible and skull exhibited less variation from the averaged value ($p<0.01$, Table 1). The lumbar spine and the irradiated regions (i.e. femur and tibia) appeared to have higher variation ($p<0.1$, Table 1). NaF uptake significantly increased among all the regions on day 3 after radiation ($p=0.0314$, Fig. 3C). Individual variation in NaF uptake was greater than for FDG. Three mice exhibited large increases (>2.0); two mice had moderate increases, and one slightly decreased. The uptake trend was similar before and after radiation (Fig. 3D).

Systemic in ammatory reaction

Radiation significantly reduced serum IGF-1 (Fig. 4, $p<0.01$). IL-6 ($p=0.06$) showed a trend for increases after radiation, while there were no statistically significant differences in TNFα, IFNγ, IL-10 and CXCL 1. Statistical calculation of IL-12 p70 and IL-1β could not be performed because most of the measurements were below the detection limit of the assay.

Discussion

Longitudinal non-invasive functional imaging with dual isotope micro-PET/CT following local irradiation in BALB/c mice revealed regional heterogeneity in marrow and bone metabolic function. Regional changes in marrow metabolic and mineral remodeling with a concurrent abscopal effect early following radiation at a variety of sites were observed longitudinally. This is the first report to characterize functional heterogeneity and changes from medically relevant radiation exposure in the whole skeleton. The application of dual isotope strategies allowed monitoring both local and distant effects on the entire skeleton following targeted radiation, including the simultaneous functional assessment of two distinct but interdependent tissues compartments (i.e. marrow and bone). This technique may permit investigations into the multi factorial communication pathways between the two active tissue components in skeletal metabolism.

A previous study with clinical-PET showed that FDG can identify hematologically active bone marrow at specific sites [17]; another investigation employing NaF demonstrated differences in bone metabolism in two regions following treatment [2]. These reports, however, investigated only limited skeletal regions. Heterogeneity in bone uptake by FDG and NaF indicates functional differentiation among skeletal regions, suggesting metabolic differences at distinct bone sites. This heterogeneity could be due to structural and functional differences [18,19]. A greater trabecular network and less marrow volume in the spinal bones may lead to greater cross sectional area with a consequently higher metabolic activity. Previous studies have demonstrated site-specific molecular regulation involving the coordination of multiple genes [19], mirroring developmental origin of each bone in the skeleton (i.e. ‘epigenetic postcode’) [20]. This has been previously demonstrated for calvarial osteoblasts when compared to appendicular trabecular osteoblasts.Understanding regional functional differences in the skeleton may therefore be crucial for: a) mapping sections of the skeleton to identify the regions that are most affected by disease or clinical intervention rather than random selection of skeletal regions to assay, b) beginning to understand the role that local and whole body skeletal environments may play while interacting with systemic endocrine and immune elements, and c) developing treatment plans and evaluating the resulting response to disease management that incorporate factors such skeletal site and bone marrow composition.

FDG and NaF uptake of the irradiated region were significantly affected by treatment in the current investigation. Radiation decreased FDG uptake, likely indicating decreased bone marrow metabolism since the absolute number of bone marrow cells and their activity may affect FDG uptake [12]. This is in conformity with our previous report of a significant reduction in bone marrow cellularity by day 3 after radiation [9]. The early increase in NaF uptake after radiation was concomitant with a significant increase in marrow sinusoid and

endosteal lining cells, which are ultimately responsible for appositional bone formation to the endosteum, in the skeleton employing a related experimental model [9]. Endosteal lining cells, i.e. committed quiescent osteoblasts, communicate with and are precursors to the osteocyte population embedded within the mineralized matrix. These cells likely regulate the influx and efflux of mineral ions and proteins into and out of the bone extracellular space, thereby serving as a kind of blood-bone barrier/interface [21]. Increases following radiation would then elevate NaF uptake in conjunction with increases in blood volume and interstitial fluids. While committed pre-osteoblasts respond to radiation damage by increased osteocalcin synthesis, the more pluripotent mesenchymal stem cell (MSC) population within the marrow space may respond to radiation damage by differentiating into adipocytes. We have observed some evidence of this indicated by increased PPARγ gene expression in whole bone marrow following radiation, (data not shown). This could explain the consistently observed increase in marrow adiposity after day 5 in mice exposed to sublethal doses of radiation or following a localized radiation exposure. Alternatively, radiation may induce cellular senescence in bone lining cells thereby leading to a secretory phenotype (including IL-6 and TNFα) that could alter MSC lineage allocation.

Radiation may also lead to long term impairment in skeletal structure and function. Our previously reported study found diminished bone structure in long-term follow up after radiation [7]. Furthermore, there are likely biochemical and physical interactions between the bone surface (namely quiescent osteoblasts) and the adjacent marrow which may influence the radiation effects [22]. Dual isotope micro-PET/CT could be a tool to develop a comprehensive understanding of radiation-induced effects on skeletal metabolism by investigating the temporal (short- and long-term) and spatial (local vs distant) effects of radiation on bone structure and function.

An abscopal effect could result from immune system activation via cytokines elevated by radiation [23]. Irradiation to the abdomen of mice resulted in a suppression of bone marrow with increased synthesis of reactive oxygen species (ROS) in the shielded femur [24]. This observation may relate to the observed decreased FDG uptake to the non-irradiated sites. Increased vascular permeability in the non-irradiated region has also been reported [25]. Altered cytokine synthesis may therefore provide a potential mechanism explaining early increase in NaF uptake in non-irradiated regions since IL-6 increases vascular permeability [26]. Significant increases in serum CXCL 1 have been observed on day 3 after radiation [27]. This peptide is known to activate neutrophil populations, and may contribute to increases in ROS [28] and vascular permeability [29]. Investigating focused radiation-induced changes at distant skeletal regions would facilitate an understanding of plausible microenviromental changes in bone which would be favorable for potential distant bone metastases [30,31].

A potential mechanism for the radiation effect on both the osteoblast and osteoclast population in local and distant sites is described in Fig. 5. Local radiation induces inflammation in irradiated bone by activating phagocytes. ROS directly generated by radiation, and secondarily by IL-6 and neutrophils, may be partly responsible for marrow damage. IL-6, CXCL 1 and ROS can cause vascular permeability thereby altering the movement of intercellular fluids. IGF-1, IL-6 and ROS may induce bone resorption via the

activation of osteoclasts [32–34]. In our study we found higher IL-6 levels post radiation although we also observed diminished serum IGF-1 levels. These changes may lead to greater bone resorption and impaired bone formation, a recipe for significant bone loss in the irradiated area [9,7,35] and at non-irradiated skeletal sites [3]. As noted, radiation may also enhance commitment of stromal marrow (i.e. pluripotent MSCs) to adipocytes differentiation and thus reduce long-term osteogenic potential [9].

There are challenges to performing longitudinal studies in preclinical model. Repeated scans of the same animal impact anesthetic tolerance. Careful management of anesthetic delivery and plane of anesthesia are essential steps to maintain quality of data integrity. Damage to the tail vein due to repeated injections should be avoided by varying injection sites. Single time point evaluations and radiation doses may have demonstrated a small set of cytokines that are activated after radiation. Further studies with additional time points and radiation doses will clarify the role of other pro- and anti-inflammatory cytokines in skeletal damage.

Conclusions

Non-invasive longitudinal imaging with dual isotope micro-PET/CT is feasible and allows the investigation of simultaneous changes in marrow and bone metabolic function. This technique may be useful for monitoring local and distal skeletal sites in response to radiation injury. There appears to be some functional skeletal heterogeneity among marrow and bone tissues. We observed temporally-related longitudinal changes in marrow metabolic and mineral remodeling locally and abscopally in response to local radiation injury. Molecular and biochemical mechanisms will be further investigated.

Acknowledgments

This work was supported by the National Institutes of Health (1R01CA154491-01, 1R03AR055333-01A1 and 1K12-HD055887-01) and Japan Society for the Promotion of Science Core to Core Program (23003). This work was also supported by PHS Cancer Center Support Grant P30 CA77398 and the Joseph E.Wargo cancer research fund from the University of Minnesota. Dr. Clifford J. Rosen received funding support from the National Institutes of Health (R24DK092759). The authors acknowledge and thank Dr. Kihak Lee (Siemens Medical Solutions, Knoxville, TN, USA) for advice and fruitful discussion pertaining to this experiment and report, Dr. Bruce E. Hammer (Center for Magnetic Recording Research, Minneapolis, MN, USA) for his help with the Siemens micro-PET/CT scanner, and Phuong T. Le (Maine Medical Center Research Institute, Scarborough, ME, USA) for the measurement of pro-inflammatory markers.

References

1. Siegel R, DeSantis C, Virgo K, Stein K, Mariotto A, Smith T, Cooper D, Gansler T, Lerro C, Fedewa S. Cancer treatment and survivorship statistics, 2012. CA Cancer J Clin. 2012; 62 (4):220–241. [PubMed: 22700443]
2. Frost ML, Blake GM, Cook GJ, Marsden PK, Fogelman I. Differences in regional bone perfusion and turnover between lumbar spine and distal humerus:< sup> 18 F-fluoride PET study of treatment-naïve and treated postmenopausal women. Bone. 2009; 45 (5):942–948. [PubMed: 19660584]
3. Hui SK, Khalil A, Zhang Y, Coghill K, Le C, Dusenbery K, Froelich J, Yee D, Downs L. Longitudinal assessment of bone loss from diagnostic computed tomography scans in gynecologic cancer patients treated with chemotherapy and radiation. Am J Obstet Gynecol. 2010; 203 (4):353, e351–e357. [PubMed: 20684943]

4. Bolan PJ, Arentsen L, Sueblinvong T, Zhang Y, Moeller S, Carter JS, Downs LS, Ghebre R, Yee D, Froelich J. Water–fat MRI for assessing changes in bone marrow composition due to radiation and chemotherapy in gynecologic cancer patients. J Magn Reson Imaging. 2013
5. Chityala R, Pudipeddi S, Arensten L, Hui S. Segmentation and Visualization of a Large, High-Resolution Micro-CT Data of Mice. J Digit Imaging. 2013:1–7. [PubMed: 22992868]
6. Huchet A, Belkacémi Y, Frick J, Prat M, Muresan-Kloos I, Altan D, Chapel A, Gorin NC, Gourmelon P, Bertho JM. Plasma Flt-3 ligand concentration correlated with radiation-induced bone marrow damage during local fractionated radiotherapy. International Journal of Radiation Oncology* Biology* Physics. 2003; 57 (2):508–515.
7. Hui SK, Fairchild GR, Kidder LS, Sharma M, Bhattacharya M, Jackson S, Le C, Petryk A, Islam MS, Yee D. The Influence of Therapeutic Radiation on the Patterns of Bone Remodeling in Ovary-Intact and Ovariectomized Mice. Calcif Tissue Int. 2013:1–13.
8. Nielsen OS, Munro A, Tannock I. Bone metastases: pathophysiology and management policy. J Clin Oncol. 1991; 9 (3):509–524. [PubMed: 1705581]
9. Hui SK, Sharkey L, Kidder LS, Zhang Y, Fairchild G, Coghill K, Xian CJ, Yee D. The influence of therapeutic radiation on the patterns of bone marrow in ovary-intact and ovariectomized mice. PloS one. 2012; 7 (8):e42668. [PubMed: 22880075]
10. Bianco P. Minireview: The Stem Cell Next Door: Skeletal and Hematopoietic Stem Cell “Niches” in Bone. Endocrinology. 2011; 152 (8):2957–2962. [PubMed: 21610157]
11. Fowler J. Development of radiobiology for oncology-a personal view. Phys Med Biol. 2006; 51 (13):R263–R286. [PubMed: 16790907]
12. Higashi T, Fisher SJ, Brown RS, Nakada K, Walter GL, Wahl RL. Evaluation of the early effect of local irradiation on normal rodent bone marrow metabolism using FDG: preclinical PET studies. J Nucl Med. 2000; 41 (12):2026–2035. [PubMed: 11138688]
13. Czernin J, Satyamurthy N, Schiepers C. Molecular Mechanisms of Bone 18F-NaF Deposition. J Nucl Med. 2010; 51 (12):1826. [PubMed: 21078790]
14. Feng B, Yan S, Chen M, Austin DW, Deng J, Mintzer RA. Automated least-squares calibration of the coregistration parameters for a micro PET-CT system. Nuclear Science, IEEE Transactions on. 2011; 58 (5):2303–2307.
15. Wu H-M, Sui G, Lee C-C, Prins ML, Ladno W, Lin H-D, Amy SY, Phelps ME, Huang S-C. In vivo quantitation of glucose metabolism in mice using small-animal PET and a microfluidic device. J Nucl Med. 2007; 48 (5):837–845. [PubMed: 17475972]
16. Hawkins RA, Choi Y, Huang SC, Hoh CK, Dahlbom M, Schiepers C, Satyamurthy N, Barrio JR, Phelps ME. Evaluation of the skeletal kinetics of fluorine-18-fluoride ion with PET. J Nucl Med. 1992; 33 (5):633–642. [PubMed: 1569473]
17. Rose BS, Liang Y, Lau SK, Jensen LG, Yashar CM, Hoh CK, Mell LK. Correlation Between Radiation Dose to< sup> 18 F-FDG-PET Defined Active Bone Marrow Subregions and Acute Hematologic Toxicity in Cervical Cancer Patients Treated With Chemoradiotherapy. International Journal of Radiation Oncology* Biology* Physics. 2012; 83 (4):1185–1191.
18. Ritman EL, Bolander ME, Fitzpatrick LA, Turner RT. Micro-CT imaging of structure-to-function relationship of bone microstructure and associated vascular involvement. Technol Health Care. 1998; 6 (5):403–412. [PubMed: 10100942]
19. Turner CH, Hsieh YF, Müller R, Bouxsein ML, Rosen CJ, McCrann ME, Donahue LR, Beamer WG. Variation in bone biomechanical properties, microstructure, and density in BXH recombinant inbred mice. J Bone Miner Res. 2001; 16 (2):206–213. [PubMed: 11204420]
20. Rawlinson SC, McKay IJ, Ghuman M, Wellmann C, Ryan P, Prajaneh S, Zaman G, Hughes FJ, Kingsmill VJ. Adult rat bones maintain distinct regionalized expression of markers associated with their development. PloS one. 2009; 4 (12):e8358. [PubMed: 20027296]
21. Dobnig H, Turner R. Evidence that intermittent treatment with parathyroid hormone increases bone formation in adult rats by activation of bone lining cells. Endocrinology. 1995; 136 (8):3632–3638. [PubMed: 7628403]
22. Poncin G, Beaulieu A, Humblet C, Thiry A, Oda K, Boniver J, Defresne M-P. Characterization of spontaneous bone marrow recovery after sublethal total body irradiation: importance of the osteoblastic/adipocytic balance. PloS one. 2012; 7 (2):e30818. [PubMed: 22363493]

23. Prise KM, O'Sullivan JM. Radiation-induced bystander signalling in cancer therapy. Nature Reviews Cancer. 2009; 9 (5):351–360.
24. Jia D, Koonce NA, Griffin RJ, Jackson C, Corry PM. Prevention and mitigation of acute death of mice after abdominal irradiation by the antioxidant N-acetyl-cysteine (NAC). Radiat Res. 2010; 173 (5):579–589. [PubMed: 20426657]
25. Ullrich R, Casarett G. Interrelationship between the early inflammatory response and subsequent fibrosis after radiation exposure. Radiat Res. 1977; 72 (1):107–121. [PubMed: 905507]
26. Maruo N, Morita I, Shirao M, Murota S. IL-6 increases endothelial permeability in vitro. Endocrinology. 1992; 131 (2):710–714. [PubMed: 1639018]
27. Van der Meeren A, Monti P, Vandamme M, Squiban C, Wysocki J, Griffiths N. Abdominal radiation exposure elicits inflammatory responses and abscopal effects in the lungs of mice. Radiat Res. 2005; 163 (2):144–152. [PubMed: 15658889]
28. Babior BM. Oxygen-dependent microbial killing by phagocytes (second of two parts). The New England journal of medicine. 1978; 298 (13):721. [PubMed: 203852]
29. Lei X, Hossain M, Qadri SM, Liu L. Different microvascular permeability responses elicited by the CXC chemokines MIP-2 and KC during leukocyte recruitment: role of LSP1. Biochem Biophys Res Commun. 2012; 423 (3):484–489. [PubMed: 22683630]
30. Joyce JA, Pollard JW. Microenvironmental regulation of metastasis. Nature Reviews Cancer. 2008; 9 (4):239–252.
31. Camphausen K, Moses MA, Beecken W-D, Khan MK, Folkman J, O'Reilly MS. Radiation therapy to a primary tumor accelerates metastatic growth in mice. Cancer Res. 2001; 61 (5):2207–2211. [PubMed: 11280788]
32. Rosen CJ. Circulating IGF-I and bone remodeling: New insights into old questions. IBMS BoneKEy. 2008; 5 (1):7–15.
33. Ishimi Y, Miyaura C, Jin CH, Akatsu T, Abe E, Nakamura Y, Yamaguchi A, Yoshiki S, Matsuda T, Hirano T. IL-6 is produced by osteoblasts and induces bone resorption. The Journal of Immunology. 1990; 145 (10):3297–3303. [PubMed: 2121824]
34. Garrett I, Boyce B, Oreffo R, Bonewald L, Poser J, Mundy G. Oxygen-derived free radicals stimulate osteoclastic bone resorption in rodent bone in vitro and in vivo. J Clin Invest. 1990; 85 (3):632. [PubMed: 2312718]
35. Hotta M, Fukuda I, Sato K, Hizuka N, Shibasaki T, Takano K. The relationship between bone turnover and body weight, serum insulin-like growth factor (IGF) I, and serum IGF-binding protein levels in patients with anorexia nervosa. J Clin Endocrinol Metab. 2000; 85 (1):200–206. [PubMed: 10634387]

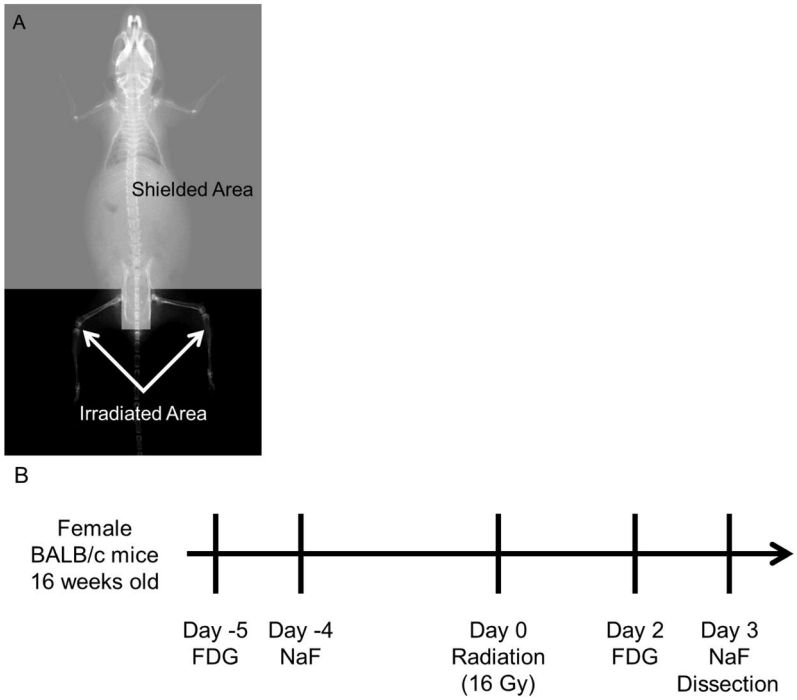

Fig. 1.

(A) Shielding designed to deliver radiation to the hind limbs. (B) Schematic of the experimental design. Micro-PET/CT acquisition was performed serially with FDG and NaF before and after the radiation to the same mice. Mice were dissected on day 3 after the radiation.

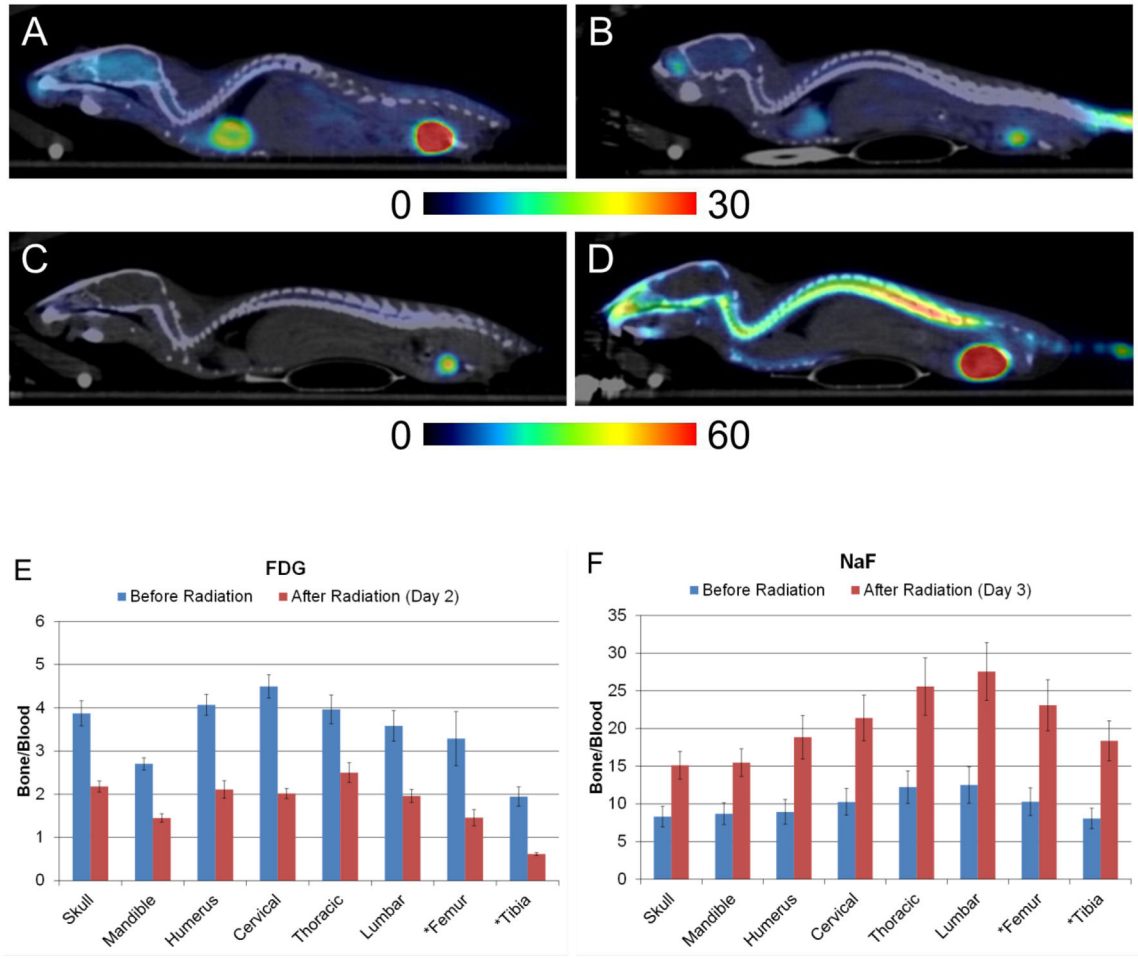

Fig. 2.

FDG uptake before(A) and after radiation(B). NaF uptake before radiation(C) and after radiation(D). Constant maximum and minimum intensities are set in the images for each tracer. (E) FDG uptake before (blue bars, $p<0.0001$) and after (red bars, $p=0.0002$) radiation is significantly different among bone regions. (F) NaF uptake before (blue bars, $p<0.0001$) and after (red bars, $p=0.0003$) radiation is significantly different. Star(*) indicates irradiated bony region.

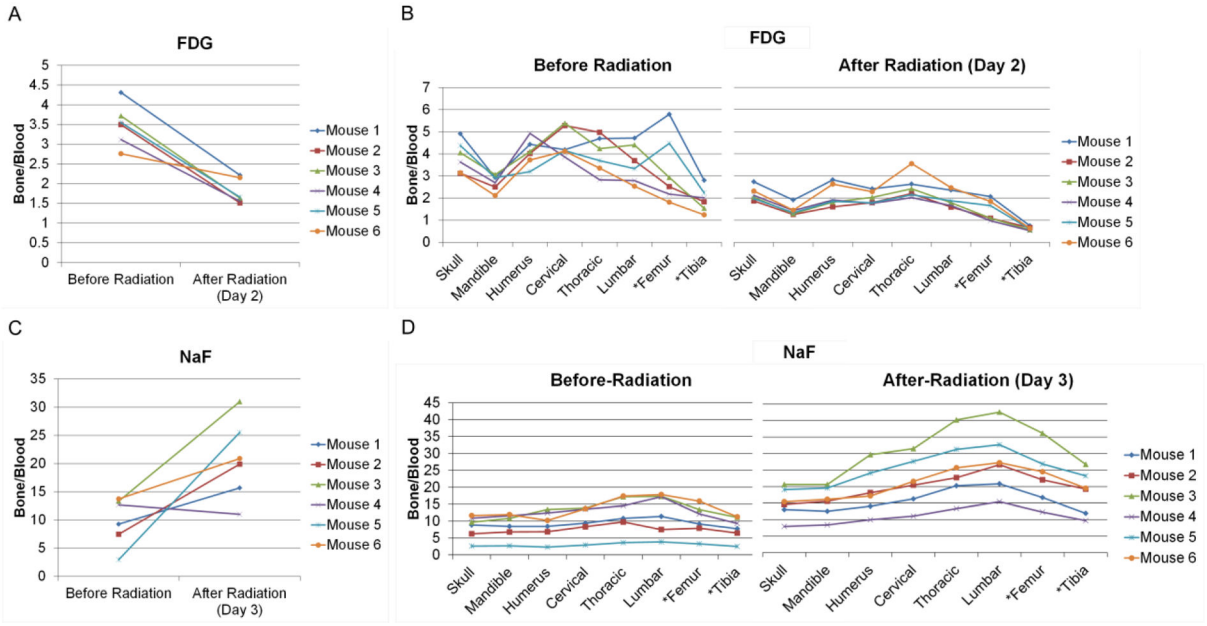

Fig. 3.

Radiation response pattern on individual mouse marrow and bone metabolism. (A) Radiation decreases FDG uptake over all regions ($p<0.0001$) on day 2 after radiation. (B) FDG uptake before and after radiation among eight different bone regions. (C) Radiation significantly increased NaF uptake among all the regions on day 3 after the radiation ($p=0.0314$). (D) NaF uptake before and after radiation among the bony regions. Star(*) indicates irradiated bony region.

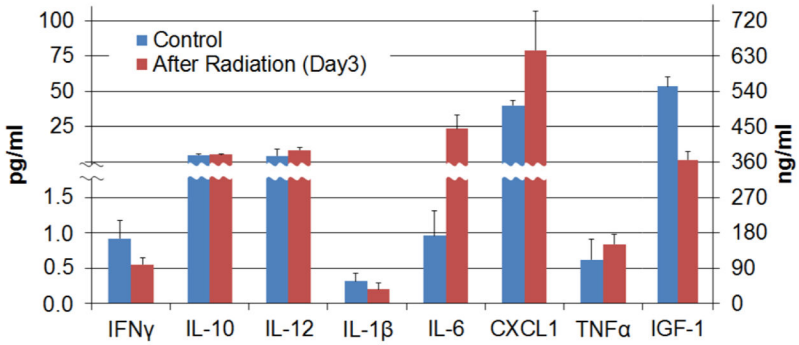

	IFNγ	IL-10	IL-12	IL-1β	IL-6	CXCL1	TNFα	IGF-1
Difference (Radiation - Control)	-0.37	0.29	3.97	-0.12	19.78	39.02	0.42	-186.50
95% CI lower	-1.01	-2.04	NC	NC	-1.27	-28.43	-0.19	-258.70
95% CI upper	0.28	2.62	NC	NC	40.82	106.50	1.02	-114.20
p (two-sided t-test)	0.22	0.78	NC	NC	0.06	0.21	0.15	< 0.01

Fig. 4.

Systemic production of in ammatory mediators. The radiation group had lower mean IGF-1and higher mean IL-6. Right axis for IFG-1. NC: not calculate.

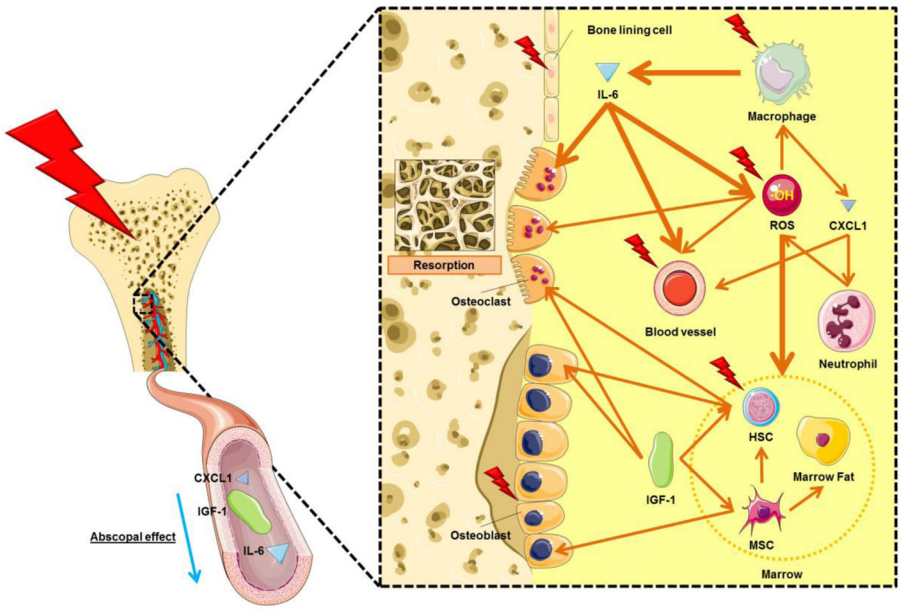

Fig. 5.

Postulated mechanisms of local and systemic damage on marrow and bone in local radiation in an early time period. Bold arrows indicate greater effect caused by source. HSC: hematopoietic stem cell. MSC: mesenchymal stem cell.

Table 1

Estimated change due to radiation. FDG averaged over all regions is expected to decrease to 50% of its pre-radiation level. This effect varied by region, and was particularly low for the tibia, where post-radiation FDG was 32% of its pre-radiation level. The NaF level averaged over all regions is expected to increase by a factor of 2.2 following radiation. However, this increase varied by region, from a factor of 1.9 in the skull and mandible to a factor of 2.4 in the femur and tibia. The wide confidence intervals are the result of variable effects seen in different mice (see Fig. 3C).

	FDG			NaF		
Skeletal regions	**Ratio before/after (day 2) radiation**	**95% CI lower**	**95% CI upper**	**Ratio before/after (day 3) radiation**	**95% CI lower**	**95% CI upper**
Skull	0.57	0.44	0.72	1.9‡	1.0	3.6
Mandible	0.53	0.42	0.68	1.9‡	1.0	3.6
Humerus	0.51	0.40	0.65	2.3	1.2	4.3
Cervical	0.45	0.35	0.57	2.2	1.2	4.2
Thoracic	0.63†	0.49	0.80	2.2	1.2	4.2
Lumbar	0.55	0.43	0.71	2.4	1.3	4.5
* Femur	0.46	0.36	0.59	2.4‖	1.3	4.5
* Tibia	0.32†	0.25	0.42	2.4‖	1.3	4.5
Overall average	0.50	0.41	0.60	2.2‖	1.1	4.5
Radiation effect to whole skeleton		< 0.0001			0.0314	
Radiation × skeletal region interaction		0.0002			0.0003	

* Irradiated region.

Model contrasts:

† For FDG, thoracic spine had a higher ratio and tibia had a lower ratio compared to the overall average ($p<0.01$).

‡ For NaF, mandible and skull had a lower ratio compared to the overall average ($p<0.01$).

‖ For NaF, lumbar spine, femur, and tibia had a marginally higher ratio compared to the overall average ($p<0.1$).